

^{121,123}Sb NQR as a microscopic probe in *Te* doped correlated semimetal *FeSb₂* : emergence of electronic Griffith phase, magnetism and metallic behavior

A. A. Gippius,^{1,2} S. V. Zhurenko,² R. Hu,^{3,*} C. Petrovic,³ and M. Baenitz^{1,†}

¹Max Planck Institute for Chemical Physics of Solids, 01187 Dresden, Germany.

²Faculty of Physics, M.V. Lomonosov Moscow State University, Moscow 119991, Russia.

³Condensed Matter Physics and Materials Science Department,
Brookhaven National Laboratory, Upton, New York 11973, USA.

(Dated: November 7, 2018)

^{121,123}Sb nuclear quadrupole resonance (NQR) was applied to *Fe*(*Sb*_{1-*x*}*Te*_{*x*})₂ in the low doping regime ($x = 0, 0.01$ and 0.05) as a microscopic zero field probe to study the evolution of *3d* magnetism and the emergence of metallic behavior. Whereas the NQR spectra itself reflects the degree of local disorder via the width of the individual NQR lines, the spin lattice relaxation rate (SLRR) $1/T_1(T)$ probes the fluctuations at the *Sb* - site. The fluctuations originate either from conduction electrons or from magnetic moments. In contrast to the semi metal *FeSb₂* with a clear signature of the charge and spin gap formation in $1/T_1(T)T \sim \exp/(\Delta k_B T)$, the 1% *Te* doped system exhibits almost metallic conductivity and the SLRR nicely confirms that the gap is almost filled. A weak divergence of the SLRR coefficient $1/T_1(T)T \sim T^{-n} \sim T^{-0.2}$ points towards the presence of electronic correlations towards low temperatures. This is supported by the electronic specific heat coefficient $\gamma = (C_{el}/T)$ showing a power law divergence $\gamma(T) \sim T^{-m} \sim (1/T_1 T)^{1/2} \sim T^{-n/2} \sim C_{el}/T$ which is expected in the renormalized Landau Fermi liquid theory for correlated electrons. In contrast to that the 5% *Te* doped sample exhibits a much larger divergence in the SLRR coefficient showing $1/T_1(T)T \sim T^{-0.72}$. According to the specific heat divergence a power law with $n = 2m = 0.56$ is expected for the SLRR. This dissimilarity originates from admixed critical magnetic fluctuations in the vicinity of antiferromagnetic long range order with $1/T_1(T)T \sim T^{-3/4}$ behaviour. Furthermore *Te*-doped *FeSb₂* as a disordered paramagnetic metal might be a platform for the electronic Griffith phase scenario. NQR evidences a substantial asymmetric broadening of the ^{121,123}Sb NQR spectrum for the 5% sample. This has purely electronic origin in agreement with the electronic Griffith phase and stems probably from an enhanced *Sb-Te* bond polarization and electronic density shift towards the *Te* atom inside *Sb-Te* dumbbell.

PACS numbers: 71.27., 71.55.Jv, 75.30.Mb, 76.60.Gv

I. INTRODUCTION

Magnetic resonance is a very suitable microscopic tool for correlated matter at the verge of long range magnetic ordering and aims in particular to expose the real nature of the magnetic fluctuations (antiferromagnetic (*afm*) - versus ferromagnetic (*fm*)) by temperature- and field-scaling¹. Local moment *4f*- and *5f*- systems driven by RKKY - and Kondo interaction could be tuned towards order through the quantum critical point (QCP) by either pressure, substitution or magnetic field²⁻⁹. Among *3d*- magnets tunable quantum criticality could be found in itinerant systems like *NbFe₂*¹⁰ and (*Ta, V*)*Fe₂*^{11,12} but also in systems with more localized *Fe* moments like *YFe₂Al₁₀*¹³ and *YbFe₂Al₁₀*¹⁴. Here in contrast to the itinerant *Fe* systems there is strong evidence for the emergence of weak Kondo interaction among the localized *Fe* moments. Signatures of Kondo type of correlations are also found in some magnetic semimetals. *FeSi*¹⁵⁻¹⁷, *FeSb₂*^{18,19} and *FeGa₃*²⁰⁻²² attracted great attention because of their non-magnetic ground state and their promising low temperature thermoelectric performance. Metallic behavior and *Fe*-based magnetism could be introduced by controlled substitutions on the *Fe*- or the framework- site. For example for *Fe*(*Ga*_{1-*x*}*Ge*_{*x*})₃ *Ga*-NQR was performed to monitor

the effect of *Ge*- substitution across the phase diagram and to probe the magnetic fluctuations at zero magnetic field via the spin lattice relaxation rate (SLRR) through the QCP. In conclusion we found an absence of induced disorder, localized antiferromagnetic Kondo-like correlations at low doping levels and critical ferromagnetic fluctuations at the QCP²². In contrast to that the *Co* substitution on the *Fe* site introduces antiferromagnetic correlations in (*Fe*_{1-*x*}*Co*_{*x*})*Ga₃* but with sizable induced disorder^{21,23}. Along this line we started to work on *Sb* NQR in *Fe*(*Sb*_{1-*x*}*Te*_{*x*})₂ where in contrast to *Fe*(*Ga*_{1-*x*}*Ge*_{*x*})₃ an electronic Griffith phase is predicted for the disordered paramagnetic metal at the verge of canted antiferromagnetism^{24,25}. Being a local probe at zero field NQR could capture both most relevant points a) the degree of disorder b) the onset of critical antiferromagnetic fluctuations at the verge of long range order. Furthermore NQR might be of use to disentangle the electronic from the magnetic Griffith phase⁹. In the correlated electron metal picture the SLRR is strongly related to the specific heat coefficient γ via $1/T_1 T \sim N^2(E_F) \sim \gamma^2 \equiv (C/T)^2$ (Korringa law¹). For weak itinerant metals the Moriya- and the Herz Millis theory captures many different cases and systems²⁶⁻²⁸. Especially at the verge to long range magnetic order power laws for the SLRR are predicted $(1/T_1(T)T \sim T^{-3/4}$ (*afm*) $\sim T^{-4/3}$ (*fm*)²⁶⁻²⁸

). Frequently non Fermi liquid behavior (NFL) was found for many systems which frequently originates from by local disorder. Disorder induced NFL behavior is discussed for many $3d$ - and $4f$ - and $5f$ - system⁹. Here for itinerant $3d$ systems (and to some extent U - based $5f$ systems) the Griffith phase was established^{9,29-32} whereas for some more localized $4f$ Kondo systems the Kondo glass scenario was proposed to capture the effect of disorder on the bulk properties³³. So far detailed microscopic studies like NMR or μ SR in quantum critical itinerant d electron semimetals on the local effect of doping and the evolution of an electronic Griffith phase are missing. Here we report the results of $^{121,123}\text{Sb}$ NQR spectroscopy and nuclear spin-lattice relaxation (SLR) $1/T_1$ experiments on the correlated semimetal FeSb_2 and the Te doped systems $\text{Fe}(\text{Sb}_{0.99}\text{Te}_{0.01})_2$ and $\text{Fe}(\text{Sb}_{0.95}\text{Te}_{0.05})_2$.

II. EXPERIMENTAL

Single crystals of $\text{Fe}(\text{Sb}_{1-x}\text{Te}_x)_2$ ($x = 0.01, 0.05$) were prepared as described in²⁴. For NQR measurements $\text{Fe}(\text{Sb}_{1-x}\text{Te}_x)_2$ single crystals which exhibit good metallic conductivity already at $x = 0.01$ ²⁴ were crushed into fine powder and mixed with paraffin. NQR experiments were performed using phase-coherent pulsed Tecmag-Apollo NMR spectrometer. $^{121,123}\text{Sb}$ NQR spectra were measured using a frequency step point-by-point spin-echo technique at 4.2 K by integration of the spin-echo envelope in the time domain and averaging over scan accumulation number which depends on the sample. The ^{123}Sb nuclear spin-lattice relaxation was measured using the saturation recovery method in the temperature range of 2.5 - 200 K. In addition, low temperature specific heat measurements were carried out on $\text{Fe}(\text{Sb}_{1-x}\text{Te}_x)_2$ ($x = 0.01, 0.05$) single crystals using the Quantum Design PPMS in the temperature range of 0.5 - 30 K.

III. RESULTS

A. $^{121,123}\text{Sb}$ NQR spectra

Bulk measurements reported previously^{24,25} provide only macroscopic evidence for the emergence of an electronic Griffith phase accompanied by NFL behavior in Te -doped FeSb_2 . To obtain a microscopic insight into underlying physics of this system we performed $^{121,123}\text{Sb}$ nuclear quadrupole resonance (NQR) spectroscopy study on the same $\text{Fe}(\text{Sb}_{1-x}\text{Te}_x)_2$ ($x = 0.01, 0.05$) samples. $^{121,123}\text{Sb}$ NQR spectra measured at 4.2 K for both samples are presented in Fig.1 together with the spectrum of the undoped FeSb_2 at 10 K adopted from¹⁹. As seen from this figure even a very small (1%) Te doping causes significant broadening of the Sb NQR lines. Moreover, ^{121}Sb ν_1 line (58.5 MHz; $|\pm 1/2\rangle \leftrightarrow |\pm 3/2\rangle$ transition) and ^{123}Sb ν_2 line (55.8 MHz; $|\pm 1/2\rangle \leftrightarrow |\pm 3/2\rangle$ transition) already start to overlap in the $\text{Fe}(\text{Sb}_{1-x}\text{Te}_x)_2$

($x = 0.01$) compound. Further increase of Te doping ($x=0.05$) leads to complete overlapping of these two NQR lines and formation of two broad shoulders to the left from ^{123}Sb ν_2 NQR line. Similar asymmetric broadening with formation of a low frequency shoulder is exhibited by all other $^{121,123}\text{Sb}$ NQR transition lines in the $\text{Fe}(\text{Sb}_{0.95}\text{Te}_{0.05})_2$ sample (see Fig.1, upper panel).

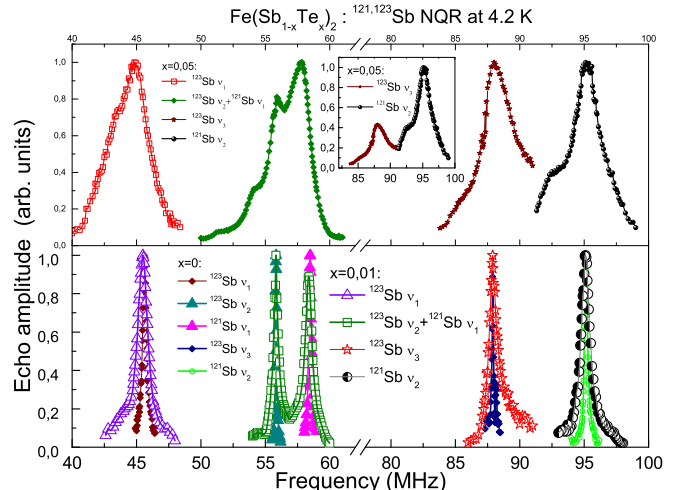


FIG. 1. (color online). $^{121,123}\text{Sb}$ spectra measured at 4.2 K in $\text{Fe}(\text{Sb}_{1-x}\text{Te}_x)_2$ compounds with $x = 0.01$ (lower panel) and 0.05 (upper panel). For comparison, the same Sb NQR lines for the undoped FeSb_2 measured at 10 K and retrieved from¹⁹ are presented (lower panel). The intensities of all transitions except ν_2 line (55.9 MHz; $|\pm 3/2\rangle \leftrightarrow |\pm 5/2\rangle$ transition) for the $\text{Fe}(\text{Sb}_{0.95}\text{Te}_{0.05})_2$ sample are normalized on their maximum intensity values. Inset: ^{123}Sb ν_3 line (88.0 MHz; $|\pm 5/2\rangle \leftrightarrow |\pm 7/2\rangle$ transition) and ^{122}Sb ν_2 line (95.1 MHz; $|\pm 5/2\rangle \leftrightarrow |\pm 7/2\rangle$ transition) without normalization for the $\text{Fe}(\text{Sb}_{0.95}\text{Te}_{0.05})_2$ sample. Solid lines are guides for eye.

The full width at half maximum (FWHM) for ^{123}Sb ν_1 line (44.85 MHz; $|\pm 1/2\rangle \leftrightarrow |\pm 3/2\rangle$ transition) amounts 0.45 MHz, 0.91 MHz and 3.63 MHz for the Te concentration $x = 0, 0.01$ and 0.05 , respectively. In other words, *only* 5% of heterovalent doping of Te for Sb results in almost one order of magnitude Sb NQR line broadening which is rather substantial. For comparison, 5% of Co substitution for Fe in relative to FeSb_2 nonmagnetic Kondo-like semiconductor FeGa_3 causes increasing of ^{69}Ga ($I=3/2$) NQR FWHM from 0.044 MHz to 0.18 MHz³⁴ which is factor of 2 less than that in FeSb_2 . Unfortunately, we were not able to estimate FWHM values for other $^{121,123}\text{Sb}$ NQR lines due to line overlapping in the $\text{Fe}(\text{Sb}_{0.95}\text{Te}_{0.05})_2$ sample. In order to extract quantitative information from experimental $^{121,123}\text{Sb}$ NQR spectra we determined the line width at 80% level from maximum line intensity. The obtained values are listed in Table 1 demonstrating considerable increase in $^{121,123}\text{Sb}$ NQR line width in FeSb_2 with Te doping.

TABLE I. Width of the $^{121,123}\text{Sb}$ NQR transition lines in $\text{Fe}(\text{Sb}_{1-x}\text{Te}_x)_2$ samples determined at 80% from maximum line intensity.

$\text{Fe}(\text{Sb}_{1-x}\text{Te}_x)_2$	^{121}Sb $I = 5/2$ $\gamma/2\pi = 10.188 \text{ MHz/T}$ $Q = -0.36 \text{ Barn}$		^{123}Sb $I = 7/2$ $\gamma/2\pi = 5.517 \text{ MHz/T}$ $Q = -0.49 \text{ Barn}$		
	$\Delta\nu_1, \text{MHz}$	$\Delta\nu_2, \text{MHz}$	$\Delta\nu_1, \text{MHz}$	$\Delta\nu_2, \text{MHz}$	$\Delta\nu_3, \text{MHz}$
$x = 0$	0.11	0.14	0.19	0.07	0.06
$x = 0.01$	0.34	0.38	0.49	0.13	0.30
$x = 0.05$	1.39	1.17	1.53	—	1.48

B. ^{123}Sb nuclear spin-lattice relaxation

To probe the effect of small Te doping on the dynamical properties of FeSb_2 system we performed ^{123}Sb nuclear spin-lattice relaxation (SLR) measurements at ^{123}Sb ν_2 NQR line ($|\pm 3/2\rangle \leftrightarrow |\pm 5/2\rangle$ transition) as a function of temperature in the range of 2.5 - 200 K by means of saturation recovery method. We have selected this line to enable comparison with the SLR data for the undoped FeSb_2 semiconductor available only for ^{123}Sb ν_2 NQR line¹⁹. Since only one NQR transition line was saturated, the ^{123}Sb ($I = 7/2$) magnetization recovery curves for $\text{Fe}(\text{Sb}_{1-x}\text{Te}_x)_2$ ($x = 0.01, 0.05$) samples were fitted by the sum of three stretched exponents^{19,35}:

$$M(\tau) = M_0 + \sum_{i=1}^3 C_i [1 - \exp(-(2k_i W_i \tau)^n)] \quad (1)$$

Here $M(\tau)$ is the spin-echo integrated intensity, M_0 is the remaining magnetization after the saturation comb (at $\tau \rightarrow 0$), τ is the delay time between the saturation comb and the spin-echo pulse sequence, $2W_0 = 1/T_1$ is the ^{123}Sb nuclear spin-lattice relaxation rate, $C_i(\eta)$, $k_i(\eta)$ are the weighting coefficients. The values of $C_i(\eta)$, $k_i(\eta)$ for FeSb_2 ($\eta = 0.43$) were taken from the numerical calculations³⁵ and were assumed not affected by Te doping. The stretched exponent parameter n was introduced in Eq. (1) to account for the structural disorder caused by Te doping. The examples of experimental recovery curves and their best fits to equation (1) obtained for $\text{Fe}(\text{Sb}_{1-x}\text{Te}_x)_2$ ($x = 0.01, 0.05$) samples at 4.2 K compared with that for the undoped FeSb_2 at 10 K (retrieved from¹⁹) are presented in Fig.2. As seen from this Figure, the approximation of the experimental recovery curves to equation (1) is rather good. While for binary FeSb_2 $n \equiv 1$, increasing of Te doping leads to significant decrease of the stretched exponent parameter: $n = 0.73(1)$ for $x = 0.01$ and $n = 0.64(2)$ for $x = 0.05$. This effect is a consequence of spatial distribution of $1/T_1$ values due to growing structural and magnetic disorder in FeSb_2 crystal lattice caused by Te substitution.

It is worth to mention two characteristic features seen from Fig.2. First, the remaining magnetization M_0 after the saturation comb (at $\tau \rightarrow 0$) is dramatically increasing with Te doping x : while the initial saturation is almost

perfect in the undoped FeSb_2 ($M_0 \approx 0.04$), M_0 becomes ≈ 0.3 for $x = 0.01$ and accomplishes ≈ 0.54 for $x = 0.05$. This effect reflects an extreme broadening and even overlapping of Sb NQR lines in $\text{Fe}(\text{Sb}_{1-x}\text{Te}_x)_2$ with increasing x (Fig.1). The intense spin diffusion effectively hampers saturation process despite all our efforts to optimize the saturation comb and minimize the M_0 value. The second interesting feature of the experimental data shown in Fig.2 is significant visible shift of the recovery curves towards low τ values with increasing Te doping x which indicates very fast increase of the $1/T_1$ values with increasing x . This effect also favors increasing of the remaining magnetization M_0 , as have been observed for the undoped FeSb_2 sample with increasing temperature¹⁹.

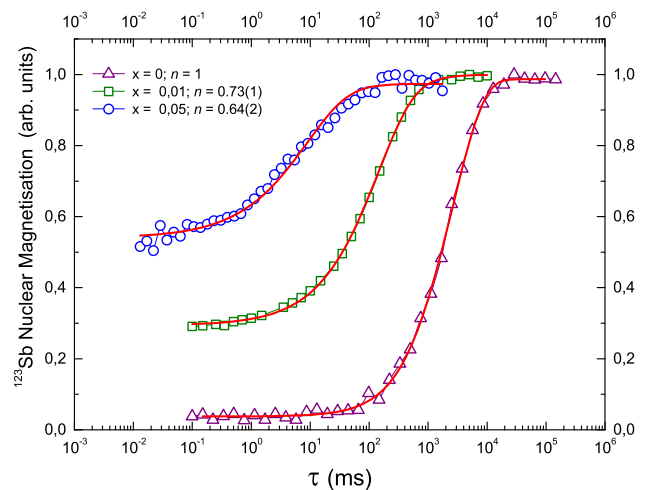


FIG. 2. (color online). ^{123}Sb magnetization recovery curves for the ν_2 NQR line (quadrupole transition $|\pm 3/2\rangle \leftrightarrow |\pm 5/2\rangle$) in the $\text{Fe}(\text{Sb}_{1-x}\text{Te}_x)_2$ ($x = 0.01, 0.05$) samples at 4.2 K and FeSb_2 at 10 K. The latter curve was adopted from Ref.¹⁹. Solid lines are the best fits to Eq.(2) with $n = 1, 0.73(1), 0.64(2)$ for $x = 0, 0.01, 0.05$, respectively.

The resulting temperature dependences of $1/T_1 T$ as a function of temperature for $\text{Fe}(\text{Sb}_{1-x}\text{Te}_x)_2$ ($x = 0, 0.01, 0.05$) samples are presented in Fig.3. As clearly seen from this figure, even low ($x = 0.01$) Te doping leads to drastic increase of the Sb NSLR in more than one order of magnitude in the low temperature range 2 - 50 K.

As has been shown in Refs.^{24,25}, even extremely low Te doping of $x = 0.001$ leads to transition from semiconducting to metallic behavior so that at $x = 0.01$ one can expect Korringa-like SLRN governed by conduction electrons. Indeed, for the $FeSb_{0.99}Te_{0.01}$ sample $1/T_1T(T)$ might be considered as almost temperature independent in the range of 2 - 70 K (Fig.3). Above 70 K $1/T_1T$ in $FeSb_{0.99}Te_{0.01}$ sample increases merging to that for the undoped $FeSb_2$.

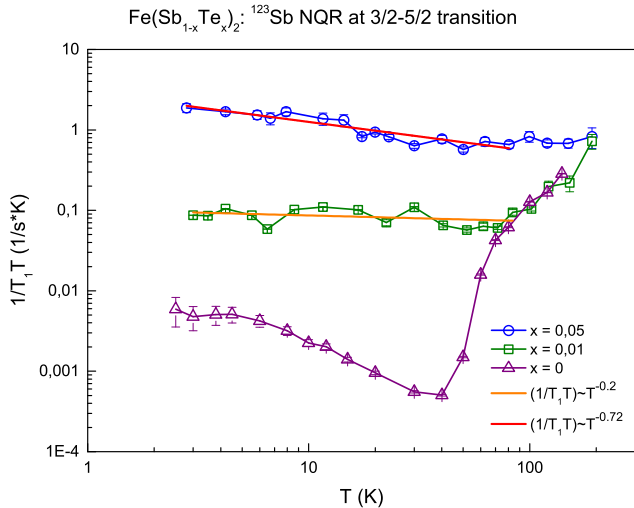


FIG. 3. (color online). $1/T_1T$ as a function of temperature for the $^{123}\text{Sb } \nu_2$ NQR line ($| \pm 3/2 \rangle \leftrightarrow | \pm 5/2 \rangle$) in $Fe(Sb_{1-x}Te_x)_2$ compounds ($x = 0, 0.01$ and 0.05). Solid straight lines are the best linear fits according to formula: $1/T_1T = a * T^{-2(1+\lambda)}$ (see text).

For the $FeSb_{0.95}Te_{0.05}$ sample where $1/T_1T$ is one order of magnitude higher than for $FeSb_{0.99}Te_{0.01}$ and a power-law divergence $1/T_1T \sim T^{-0.72}$ ($1/T_1 \sim T^{0.28}$) (Fig.3) was found towards low temperatures.

C. Specific heat

In addition to the NQR spectroscopy data we performed low temperature specific heat measurements on the same $Fe(Sb_{1-x}Te_x)_2$ ($x = 0.01, 0.05$) samples (Fig.4, upper panel). The data is in a rather good agreement with findings of Hu et al²⁵ on crystals from the same batch. Here power law divergences in $\gamma(T) = C/T$ and $\chi(T)$ are discussed in the framework of the disorder induced Griffith phase (GF) at the verge of magnetism¹⁵. According to²⁹, the low temperature divergence of specific heat in GF systems is described by power function $C(T)/T = a * T^{-1+\lambda_C}$ with $\lambda_C < 1$. Then likewise²⁵, the total low temperature behavior of specific heat in these compounds can be successfully fitted to the equation:

$$C(T)/T = \alpha * T^{-1+\lambda_C} + b * T^2 + c * T^4 \quad (2)$$

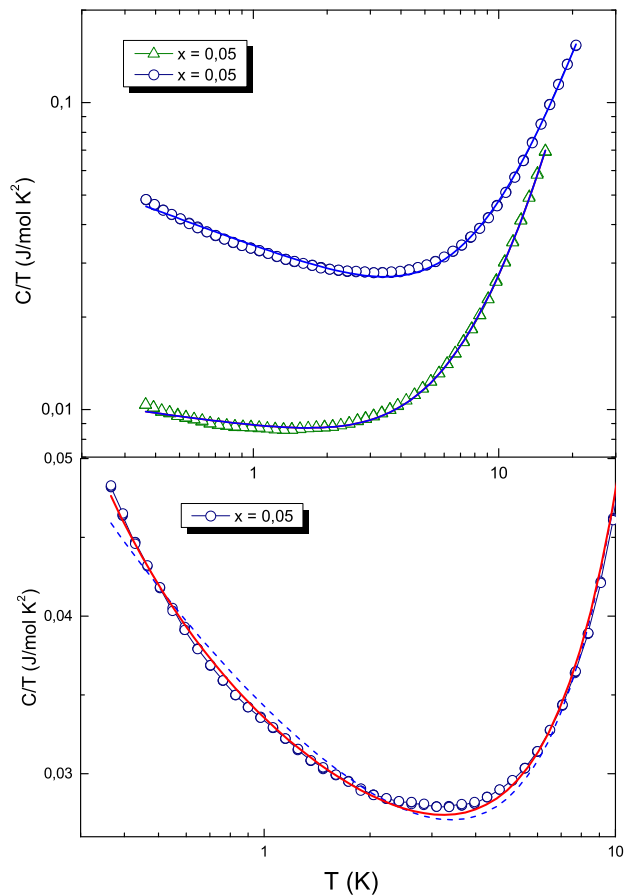


FIG. 4. (color online). Upper panel: C/T vs. T plot in $Fe(Sb_{1-x}Te_x)_2$ compounds ($x = 0.01$ and $x = 0.05$). Solid lines are the best fits to Eq. (1) (see text). Lower panel: Low temperature part of the C/T vs. T plot for the $Fe(Sb_{0.95}Te_{0.05})_2$ sample. Dashed and solid lines are the best fits to Eqn.(2) and (5), respectively.

The second and third terms in Eq.2 describes harmonic and anharmonic contributions to specific heat, respectively³⁶. The obtained values of λ_C for both samples ($\lambda_C = 0.88$ ($x = 0.01$) and 0.70 ($x = 0.05$) see tab 2) are in good agreement with that reported in Ref.²⁵.

TABLE II. Values of the parameter λ obtained from specific heat $(\lambda_{C/T})_{exp}$ and nuclear spin-lattice relaxation $(\lambda_{T_1})_{exp}$ experiments in comparison with that from Ref.², marked by (*).

x	$(\lambda_C)^*$	$(\lambda_C)_{exp}$	$(\lambda_{T_1})_{exp}$
0.01	0.91(7)	0.88(4)	0.90(6)
0.05	0.72(3)	0.70(4)	0.64(4)

IV. DISCUSSION

The origin of the observed low frequency shoulder at $^{121,123}\text{Sb}$ NQR lines can be understood as follows. With increasing of Te content x from 0.01 to 0.05 the number of hetero-dumbbells Sb-Te also increases. These dumbbells are characterized by polarization of the Sb-Te bond due to higher electronegativity of the Te atom. Therefore electronic density inside the Sb-Te dumbbell is shifted towards Te atom. As a consequence, a partial negative charge on Sb atom is reduced causing decrease of EFG followed by decreasing of Sb quadrupole frequency. At low Te concentration ($x = 0.01$) this effect is not yet visible but 5% Te seems to be enough for detection since the number of hetero-dumbbells Sb-Te increases substantially and the left shoulder on Sb NQR appears. In this simplified approach only the 1-st coordination sphere of Sb is considered which might be visualized as a Sb-Sb dumbbell with short interatomic distance ($\sim 2.8 \text{ \AA}$) surrounded by 6 Fe atoms likewise strongly distorted octahedron (Fig.5). In 5% Te substituted FeSb_2 sample one can expect appearance of hetero-dumbbell Sb-Te in the 2-nd coordination sphere of homo-dumbbell Sb-Sb which slightly reduce the charge on Sb . In conjunction with strong NQR line broadening caused by lattice disorder this explains why instead of separate peak to the left of main Sb NQR line we observe just a left shoulder.

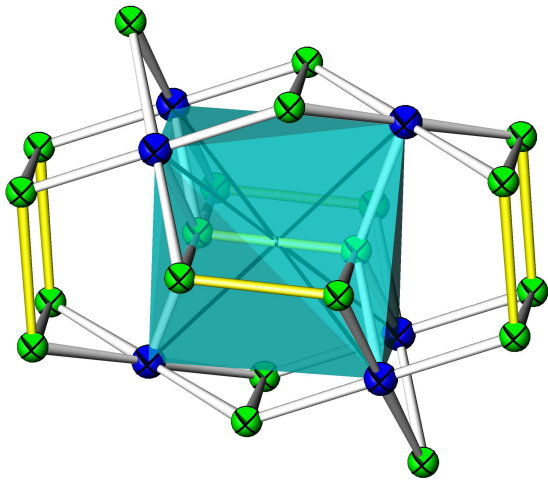


FIG. 5. (color online). Schematic illustration of the first two coordination spheres of Sb-Sb dumbbell in the FeSb_2 crystal structure. Sb atoms are indicated as green balls, Fe dark blue balls. Fe_6 octahedron surrounding the center of Sb-Sb dumbbell (black point in the center of octahedron) is indicated by green-blue.

As seen from Table 1, for all samples the broadening of the ν_1 line for ^{123}Sb isotope is higher than that for ^{121}Sb isotope in satisfactory accordance to the ratio of their quadrupole moments $^{123}Q/^{121}Q = 1.36$. This result provides an evidence of electronic quadrupole origin

rather than magnetic origin of the $^{121,123}\text{Sb}$ NQR line broadening in $\text{Fe}(\text{Sb}_{1-x}\text{Te}_x)_2$ ($x = 0.05$) sample. This supports the claim of electronic Griffith phase (EGP) in Te doped FeSb_2 and is in a strong contrast to the magnetic Griffith phase (MGP). Indeed in case of isolated magnetically ordered clusters characteristic for the magnetic Griffiths phase Sb nuclei inside these clusters should exhibit strong hyperfine magnetic fields of about $0.1 \div 1 \text{ T}$ induced from electron spins localized on Fe . Then instead of pure NQR one should observe Zeeman perturbed NQR on $^{121,123}\text{Sb}$ nuclei with pronounced splitting (or, at least, strong broadening) of initial NQR transition lines which depends on value and orientation of internal magnetic field in respect to the main EFG axes and asymmetry parameter η and is proportional to gyromagnetic ratio γ (see, for instance,³⁷). Since $^{121}\gamma/^{123}\gamma = 1.85$ broadening of ^{121}Sb NQR lines should be almost twice as for ^{123}Sb isotope. This is definitely not seen in our experimental $^{121,123}\text{Sb}$ NQR spectra in $\text{Fe}(\text{Sb}_{0.95}\text{Te}_{0.05})_2$ sample. In the upper limit of hyperfine magnetic field ($\sim 1 \text{ T}$) induced on Sb nuclei within ordered spin clusters of Griffiths phase one can even observe a "wipe-out" effect of disappearing of Sb NQR lines originated from cluster volume due to their extreme Zeeman broadening. This effect should substantially reduce the total Sb NQR intensity which was not observed in our experiment.

For a metal in the frame of the Landau Fermi liquid (LFL) the SLRR could be related to the specific heat via the density of states at the Fermi level which yields $1/T_1T \sim N^2(E_F) \sim \gamma^2 \equiv (C/T)^2 \sim T^{2(-1+\lambda)}$. Contrasting to that, if the metal is a weak itinerant magnet, the SLRR is more related to the low energy and q -averaged complex dynamic susceptibility $\chi(q,\omega)$ which yields $1/T_1T \sim \sum_q \chi(q,\omega)$. Here it matters if the correlations are fm (at $q = 0$) or afm (at $q \neq 0$). For fm correlations the SLRR is frequently found to be proportional to the bulk susceptibility $1/T_1T \sim \chi \sim T^{-1+\lambda}$ for the MGP.

For the 1% sample the specific heat coefficient power law ($m \equiv 1 - \lambda = 0.12$) suggests a SLRR power law with $n = 2m = 0.24$ which is in rather good agreement with the experimental result ($n = 0.2$). For the 5% sample the specific heat coefficient power law ($m = 0.28$) suggests a SLRR power law with $n = 2m = 0.56$ which is much smaller than what is found by experiment ($n = 0.72$). This might point towards the fact that upon doping we have a crossover from more localized correlated metal to an afm correlated itinerant metal at the verge of order. Here Moryia predicted a power law with $n = 3/4$ which is rather close to the experimental finding.

Nonetheless the specific heat coefficient enhancement factor at 2 K ($\gamma_{5\%}/\gamma_{1\%}$) is about 5 which suggests in the LFL theory an enhancement of the SLRR ($R = 1/T_1T$) ($R_{5\%}/R_{1\%}) \approx 25$ which is indeed experimentally confirmed by our spin lattice relaxation measurements.

Lets take a closer look to predictions for the SLRR in an Griffith phase. According to theoretical prediction for the magnetic Griffith phase the nuclear spin-lattice

relaxation rate should follow the equation²⁹:

$$1/T_1T(\omega, T) \propto \omega^{-2+\lambda} \tanh(\omega/T) \quad (3)$$

Since in our NQR experiment $\hbar\omega \ll k_B T$ even at lowest temperatures $\tanh(\omega/T) \approx \omega/T$ and Eq.(3) is simplified to the form:

$$1/T_1T(\omega, T) \propto \omega^{-1+\lambda}/T \propto T^{-1} \quad (4)$$

The MGP power law with $n = 1$ (assuming $\omega = \text{constant}$ in the first place) is far from the experimental values ($n = 0.2$ (for $x = 0.05$) and $n = 0.72$ (for $x = 0.05$)).

From the other hand, $\alpha \equiv 1 - n = 1/3$ is a characteristic exponent value within the Tselik and Reizer model based on scaling analysis of collective bosonic modes of the fluctuations with the spectrum $\omega \sim q^3$ near QCP providing $1/T_1T \sim T^{-2/3} \sim T^{-0.66}$ ($1/T_1 \sim T^{1/3}$) behavior at low temperatures³⁸.

The SLR results obtained for the for $Fe(Sb_{1-x}Te_x)_2$ ($x = 0.01, 0.05$) samples do not provide an unambiguous microscopic evidence in favor of either of these two models describing complicated NFL properties in the vicinity of the QCP. To gain an extra argument favoring one of these models we revisited the low temperature specific data analysis. Although approximation of specific heat experimental data by Eq. (2) is almost perfect above 5 K, the low temperature part of theoretical curve for the $x = 0.05$ sample shows systematic deviation from experimental $C(T)/T$ points which evidently diverges faster with decreasing T than power function $T^{-1+\lambda}$ (see Fig.4, lower panel). One should also take into account that more general description of NFL behavior predicts logarithmic rather than power divergence of specific heat at $T \rightarrow 0^3$. It is worth to note that the Tselik and Reizer model also predicts for the specific heat low temperature logarithmic divergence³⁸ However, $-\ln T$ function diverges even slower than $T^{-1+\lambda}$. This contradiction can be settled by implementing a dissipative quantum droplet model³⁹ which describes the critical behavior of NFL metallic magnetic systems at low $T < T^*$ below which quantum critical regime is dominated by dissipation providing stronger divergence of specific heat than the power law: $C(T)/T \propto T/\ln^2(1/T)$. Combining general logarithmic NFL divergence with even stronger divergence term of $C(T)/T \propto T/\ln^2(1/T)$ from dissipative quantum droplet model one arrives at:

$$C(T)/T = a*/T \ln^2(1/T) - b*\ln T + c*T^2 + d*T^4 \quad (5)$$

Using Eq.5 instead of Eq.2 we obtained much better agreement with experimental low temperature $C(T)/T$ data as demonstrated in Fig.4, lower panel.

V. SUMMARY

We performed a comprehensive study of correlated intermetallic system $Fe(Sb_{1-x}Te_x)_2$ ($x=0.01, 0.05$) in

the vicinity of an antiferromagnetic quantum critical point by means of NQR spectroscopy on $^{121,123}Sb$ nuclei. It was found that even a slight Tellurium doping of $x=0.05$ introduces strong lattice disorder in the binary Kondo-insulator compound $FeSb_2$ resulting in substantial asymmetric broadening Sb NQR spectrum and formation of the low frequency shoulder at left side of each of $^{121,123}Sb$ NQR transition lines due to polarization of the $Sb-Te$ bond and shifting of electronic density inside the $Sb-Te$ dumbbell towards Te atom. Furthermore the observed transformation of the Sb NQR spectrum in $Fe(Sb_{1-x}Te_x)_2$ samples are related to local changes of the electric field gradient due to the doping effect. There is no evidence for magnetic broadening of the NQR lines due to the emerging Fe – magnetism upon doping. We interpret this as the microscopic evidence for the electronic Griffith phase in strong contrast to the magnetic broadening expected for the magnetic Griffith phase.

The spin lattice relaxation results clearly show that the charge gap of the pure correlated semimetal $FeSb_2$ is filled upon Te doping. In a first approximation based on the Landau Fermi liquid theory for correlated metals the low temperature divergence of the SLRR $1/T_1T(T)$ could be scaled to the one of the specific heat coefficient $\gamma(T)$. A very good agreement was found for the 1% sample whereas the 5% sample which is closer to the antiferromagnetic ordered phase shows a significant violation of the scaling. The power law coefficient $n = 0.72$ is rather close to the one expected for antiferromagnetic criticality which is $n_{afm} = 3/4 = 0.75$. Nonetheless the enhancement factor of 5 between the $x = 0.01$ and $x = 0.05$ in the specific heat yields an enhancement of 25 in the $1/T_1T$ value which was experimentally verified. As for both samples the the specific heat divergence is in good agreement with Ref²⁵ which suggests a electronic Griffith phase the microscopic SLRR shows a remarkable lack of consistency with the magnetic Griffith phase predictions. Probably this is because of the q -averaging nature of the SLRR. Nonetheless strong evidence for antiferromagnetic critical fluctuations at zero field for the 5% Te doped $FeSb_2$ sample is given. Antiferromagnetic criticality is a rare occurrence in Fe -based systems and therefore doped Fe -based semimetals in general might provide a platform for further studies. Further more other local probes (like μ SR) should be addressed to study Griffith phase systems.

VI. ACKNOWLEDGMENTS

Authors are grateful to A. V. Shevelkov and E. A. Kravchenko for fruitful discussions, and A. V. Trofimenko for help with the experiment. A. A. Gippius and S. V. Zhurenko appreciate financial support from Russian Foundation of Basic Research (grant 16-53-52012-a). We thank H. Rave and C. Klausnitzer for technical support. Work at BNL was supported by the U.S. DOE-BES, Division of Materials Science and Engineering, under Con-

-
- * Present address: Rutgers Center for Emergent Materials and Department of Physics and Astronomy, Rutgers University, Piscataway, NJ 08854, USA.
- † corresponding author: baenitz@cpfs.mpg.de
- ¹ Y. Kuramoto and Y. Kitaoka, *Dynamics of Heavy Electrons* (Oxford University Press, New York, 2000).
 - ² S. Doniach (Plenum, New York, 1977) p. 1669.
 - ³ G. R. Stewart, *Reviews of Modern Physics* **73**, 797 (2001).
 - ⁴ P. Gegenwart, Q. Si, and F. Steglich, *Nature Physics* **4**, 186 (2008).
 - ⁵ H. v. Löhneysen, A. Rosch, M. Vojta, and P. Wölfle, *Reviews of Modern Physics* **79**, 1015 (2007).
 - ⁶ Q. Si and F. Steglich, *Science* **329**, 1161 (2010).
 - ⁷ S. Sachdev, *Quantum Phase Transitions*, 2nd ed. (Cambridge University Press, 2011).
 - ⁸ M. Brando, D. Belitz, F. Grosche, and T. Kirkpatrick, *Reviews of Modern Physics* **88**, 025006 (2016).
 - ⁹ E. Miranda and V. Dobrosavljević, *Reports on Progress in Physics* **68**, 2337 (2005).
 - ¹⁰ M. Brando, W. J. Duncan, D. Moroni-Klementowicz, C. Albrecht, D. Grüner, R. Ballou, and F. M. Grosche, *Physical Review Letters* **101**, 026401 (2008).
 - ¹¹ Y. Horie, S. Kawashima, Y. Yamada, G. Obara, and T. Nakamura, *Journal of Physics: Conference Series* **200**, 032078 (2010).
 - ¹² M. Brando, A. Kerkau, A. Todorova, Y. Yamada, P. Khuntia, T. Förster, U. Burkhard, M. Baenitz, and G. Kreiner, *Journal of the Physical Society of Japan* **85**, 084707 (2016).
 - ¹³ P. Khuntia, A. M. Strydom, L. S. Wu, M. C. Aronson, F. Steglich, and M. Baenitz, *Physical Review B* **86**, 220401 (2012).
 - ¹⁴ P. Khuntia, P. Perathepan, A. Strydom, Y. Utsumi, K.-T. Ko, K.-D. Tsuei, L. Tjeng, F. Steglich, and M. Baenitz, *Physical Review Letters* **113**, 216403 (2014).
 - ¹⁵ V. Jaccarino, G. K. Wertheim, J. H. Wernick, L. R. Walker, and S. Aarj, *Physical Review* **160**, 476 (1967).
 - ¹⁶ D. Mandrus, J. L. Sarrao, A. Migliori, J. D. Thompson, and Z. Fisk, *Physical Review B* **51**, 4763 (1995).
 - ¹⁷ N. Manyala, Y. Sidis, J. F. DiTusa, G. Aeppli, D. P. Young, and Z. Fisk, *Nature Materials* **3**, 255 (2004).
 - ¹⁸ C. Petrovic, Y. Lee, T. Vogt, N. Lazarov, S. Bud'ko, and P. Canfield, *Physical Review B* **72**, 045103 (2005).
 - ¹⁹ A. A. Gippius, M. Baenitz, K. S. Okhotnikov, S. Johnsen, B. Iversen, and A. V. Shevelkov, *Applied Magnetic Resonance* **45**, 1237 (2014).
 - ²⁰ K. Umeo, Y. Hadano, S. Narazu, T. Onimaru, M. A. Avila, and T. Takabatake, *Physical Review B* **86**, 144421 (2012).
 - ²¹ A. A. Gippius, V. Y. Verchenko, A. V. Tkachev, N. E. Gervits, C. S. Lue, A. A. Tsirlin, N. Büttgen, W. Krätschmer, M. Baenitz, M. Shatruk, and A. V. Shevelkov, *Physical Review B* **89**, 104426 (2014).
 - ²² M. Majumder, M. Wagner-Reetz, R. Cardoso-Gil, P. Gille, F. Steglich, Y. Grin, and M. Baenitz, *Physical Review B* **93**, 064410 (2016).
 - ²³ V. Verchenko, M. Likhanov, M. Kirsanova, A. Gippius, A. Tkachev, N. Gervits, A. Galeeva, N. Büttgen, W. Krätschmer, C. Lue, K. Okhotnikov, and A. Shevelkov, *Journal of Solid State Chemistry* **194**, 361 (2012).
 - ²⁴ R. Hu, V. F. Mitrović, and C. Petrovic, *Physical Review B* **79**, 064510 (2009).
 - ²⁵ R. Hu, K. Wang, H. Ryu, H. Lei, E. S. Choi, M. Uhlarz, J. Wosnitza, and C. Petrovic, *Physical Review Letters* **109**, 256401 (2012).
 - ²⁶ T. Moriya, *Spin Fluctuations in Itinerant Electron Magnetism* (Springer Berlin Heidelberg, 1985).
 - ²⁷ J. A. Hertz, *Physical Review B* **14**, 1165 (1976).
 - ²⁸ A. J. Millis, *Physical Review B* **48**, 7183 (1993).
 - ²⁹ A. H. Castro Neto, G. Castilla, and B. A. Jones, *Physical Review Letters* **81**, 3531 (1998).
 - ³⁰ R. B. Griffiths, *Physical Review Letters* **23**, 17 (1969).
 - ³¹ T. Vojta, *Journal of Low Temperature Physics* **161**, 299 (2010).
 - ³² S. Ubaid-Kassis, T. Vojta, and A. Schroeder, *Physical Review Letters* **104**, 066402 (2010).
 - ³³ T. Westerkamp, M. Deppe, R. Küchler, M. Brando, C. Geibel, P. Gegenwart, A. P. Pikul, and F. Steglich, *Physical Review Letters* **102**, 206404 (2009).
 - ³⁴ M. S. Likhanov, V. Y. Verchenko, M. A. Bykov, A. A. Tsirlin, A. A. Gippius, D. Berthebaud, A. Maignan, and A. V. Shevelkov, *Journal of Solid State Chemistry* **236**, 166 (2016).
 - ³⁵ J. Chepin and J. H. Ross, *Journal of Physics: Condensed Matter* **3**, 8103 (1991).
 - ³⁶ Cezairliya, *Specific heat of solids (Cindas Data Series on Material)* (Chem/Mats-Sci/E, 1988).
 - ³⁷ N. J. Curro, P. C. Hammel, P. G. Pagliuso, J. L. Sarrao, J. D. Thompson, and Z. Fisk, *Physical Review B* **62**, R6100 (2000).
 - ³⁸ A. M. Tselik and M. Reizer, *Physical Review B* **48**, 9887 (1993).
 - ³⁹ A. H. Castro Neto and B. A. Jones, *Physical Review B* **62**, 14975 (2000).